Acceleration of Sweeping Frequency in Eddy Current Computation

DOI:
10.1109/TMAG.2017.2688326

Document Version
Accepted author manuscript

Acceleration of Frequency Sweeping in Eddy Current Computation

Mingyang Lu, Anthony Peyton, Wuliang Yin

School of Electrical and Electronic Engineering
University of Manchester, Manchester, M13 9PL, UK
Mingyang.lu@postgrad.manchester.ac.uk
Wuliang.yin@manchester.ac.uk

Abstract **–** In this paper, a novel method for accelerating frequency sweeping in eddy current calculation using finite elements method (FEM) is presented.

Exploiting the fact that between adjacent frequencies, the eddy current distributions are similar, an algorithm is proposed to accelerate the frequency sweeping computation. The solution of the field quantities under each frequency, which involves solving a system of linear equations using the Conjugate Gradients Squared (CGS) method, is accelerated by using an optimized initial guess – the final solution from the previous frequency.

Numerical tests show that this treatment could speed up the convergence of the CGS solving process, i.e. reduced number of iterations reaching the same relative residuals or reaching smaller residuals with the same iteration number.

Keywords: Finite-element method (FEM), eddy current calculation, computation accelerating, frequency sweeping

1. Introduction

There are various electromagnetic computation techniques for eddy current simulations, such as the Finite-element method (FEM), the Boundary-element method (BEM), and the Method of Auxiliary Source (MAS) [1]. The Finite Element Method is particularly universal as it can be applied to an object of arbitrary shape and material properties. The principle of the FEM is to replace an entire continuous domain by a number of sub-domains in which the unknown function is represented by simple interpolation functions with unknown coefficients.

Based on the variation principle, the FEM transforms the boundary value problem (partial differential equation) to its corresponding variational problem. Then, the problem becomes one of solving a system of algebraic equations, of which the solution is the numerical solution of the boundary problem [2].

In recent developments, several methods have been proposed to accelerate the computation processes for eddy current calculations. These methods can be divided into two categories, namely, the improvements on electromagnetic (EM) formulation /strategy and that on the numerical solution processes.

For improvement on the formulation /strategy, a number of methods were used: a novel decomposition of the model such as ParaFEM [3, 4], multi-layered conductive structures (MCS) method [5] and second-order transmission condition (SOTC) method [6] etc. ParaFEM is a portable library of subroutines for parallel finite element analysis, which can be used for solving very large finite element problems in a range of disciplines. But this method significantly relies on the material distribution of the model. The principle of this method is decomposing the model into several individual subdomains and then solves these subdomains in parallel; however, it is worth mentioning that this method assumes weak coupling relationship between the subdomains. The multi-layered conductive structures (MCS) method is proved to be about 100 times less than conventional FEM in computation time. But, as a derivative of the Dodd and Deeds method, it can only be used for some layer-isotropic structures/models such as that encountered in pipelines, airplanes, water jet peened

components instead of arbitrary geometry models such as cracks on the structure. Second-order transmission condition (SOTC) method developed in the framework of non-conformal (NC) finite element domain decomposition method (DDM) [7], was shown to have improved accuracy on large iterations (about or over 200) but with almost no improvement on calculations with small iterations (equal or smaller than 50). FEM-BEM hybrid method [8-12] was also well used, which couples boundary-element region with finite-element region to derive solutions for in-homogenous material distributions.

For improving the numerical solution process, SuiteSparse [13] and GRID [14] were developed to improve the computation speed of solving systems of linear equations from FEM. GPU acceleration [15-18] can also increase the numerical processes by exploiting parallel computing, but at the cost of expensive hardware.

In this paper, a fast frequency-sweeping FEM method with LU decomposition and initial guess/ preconditioning is proposed, which starts from smaller relative residuals at the beginning of the iteration.

2. Methods of Edge-Element FEM Solver

After discretizing the target by using a commercial software package, in this case COMSOL, the exported file including the coordinates of the nodes, the sequence of the nodes in each element, as well as the material properties of each element can be regarded as the input of the solver, which is based on the FEM. In this part, the original Galerkin's equations are transformed into matrix form [19].

$$\int_{\Omega_c} curl\boldsymbol{N}_i \cdot vcurl\boldsymbol{A}^{(n)} d\Omega + \int_{\Omega_c} j\omega\sigma \boldsymbol{N}_i \cdot \boldsymbol{A}^{(n)} d\Omega + \int_{\Omega_c} \sigma \boldsymbol{N}_i \cdot gradV^{(n)} d\Omega = \int_{\Omega_c} curl\boldsymbol{N}_i \cdot v_0 curl\boldsymbol{A}_s d\Omega \quad (1)$$
$$i = 1, 2, ..., 6$$

$$\int_{\Omega_c} j\omega\sigma gradL_i \cdot \boldsymbol{A}^{(n)} d\Omega + \int_{\Omega_c} \sigma gradL_i \cdot gradV^{(n)} d\Omega = 0 \quad (2)$$
$$i = 1, 2, ..., 4$$

Where $\boldsymbol{N}_i$ is the vector interpolation of i^{th} edge corresponding to its nth edge element, L_i the elemental interpolation of i^{th} node corresponding to its nth element, $\boldsymbol{A}_s$ the original edge vector potential of the nth element, $\boldsymbol{A}^{(n)}$ the produced edge vector potential of the nth element, $V^{(n)}$ the electrical potential on the receiver (pick-up) coil contributed by the nth element, v the reluctivity (the reciprocal of the permeability) of the target, v_0 the reluctivity (the reciprocal of the permeability) of the air, σ the conductivity of the target.

Assuming for an arbitrary element *n*, there exist a matrix Q that can represent the stiffness matrix form of equation (1) and (2) left side for an arbitrary element.

$$Q^{(n)} = \begin{pmatrix} K^{(n)}(6\times 6) & L^{(n)}(6\times 4) \\ M^{(n)}(4\times 6) & N^{(n)}(4\times 4) \end{pmatrix} \tag{3}$$

After combining equation (3) of the whole system element, the matrix form of equation (1) and (2) can be obtained as following.

$$Q\cdot\begin{pmatrix}\begin{pmatrix} A_1 \\ \vdots \\ A_e \end{pmatrix} \\ \begin{pmatrix} V_1 \\ \vdots \\ V_o \end{pmatrix}\end{pmatrix} = \begin{pmatrix} K(e\times e) & L(e\times o) \\ M(o\times e) & N(o\times o) \end{pmatrix}\cdot\begin{pmatrix}\begin{pmatrix} A_1 \\ \vdots \\ A_e \end{pmatrix} \\ \begin{pmatrix} V_1 \\ \vdots \\ V_o \end{pmatrix}\end{pmatrix} = B \tag{4}$$

Here *K* matrix is divided into *K1* and *K2* matrix. *K1* denotes the matrix form of first vector potential related term in equation (1), which act as a fundamental formation of the vector potential. *K2* denotes the matrix form of second vector potential related term in equation (1), which exhibit the skin effect the eddy current. *L* is the matrix form of first electric potential related term in equation (1), which controls the eddy current by the Maxwell-Wagner effect- restricting the current by the shape of the target. *M* and *N* are the matrices form of first and second term in equation (2), which collectively controls the magnetostatic field part. *B* is the matrix form of the right side term of equation (1) and (2), which denotes the Dirichlet Boundary Condition. *e* and *o* represent the edge and vertex number of whole mesh respectively.

The electric field of an arbitrary element can also be derived from the vector potential and electric potential in equation (4) by using the derivative of traditional A and V-A formulation incorporating Coulomb gauge [20]:

$$\boldsymbol{E}^{(n)} = -j\omega A^{(n)} - \nabla V^{(n)} \tag{5}$$

Where $A(n)$ denotes the vector sum of the vector potential on all the edges of each tetrahedral element. $V(n)$ denotes the electric potential on all the vertex of each tetrahedral element.

Thus, the transmitter–receiver mutual inductance changes caused by the given model can also be obtained by applying the equation presented by Mortarelli (1980) or Auld and Moulder (1999). For both articles, the authors start from the Lorentz reciprocity relation and progress to reach to the same generalized equation that could be applied to any pair of coils [21]:

$$\Delta L = \frac{1}{j\omega I^2}\int_c \boldsymbol{E}_a \cdot \boldsymbol{J}_b dv = \frac{1}{j\omega I^2}\int_c \boldsymbol{E}_a \cdot \boldsymbol{E}_b \cdot \left(\sigma_a - \sigma_b\right) dv \tag{6}$$

ΔL denotes the inductance changes caused by the difference between medium *a* and *b*.

3. Accelerating Method

A. Method

Bi-conjugate Gradients Stabilised (CGS) method was used in the solution processes of Equation (4). Conventional methods start from an initial guess of a zero vector. As the solutions of the adjacent frequencies are quite similar, the solution for the previous frequency is assigned to be initial guess of the next frequency. Consequently, the iterations in each solving process start from an optimised guess / smaller residuals and thus the number of iterations would be much reduced. And the simulations are computed by ThinkStation P510 platform with Dual Intel Xeon E5-2600 v4 Processor, with 16G RAM.

B. Models

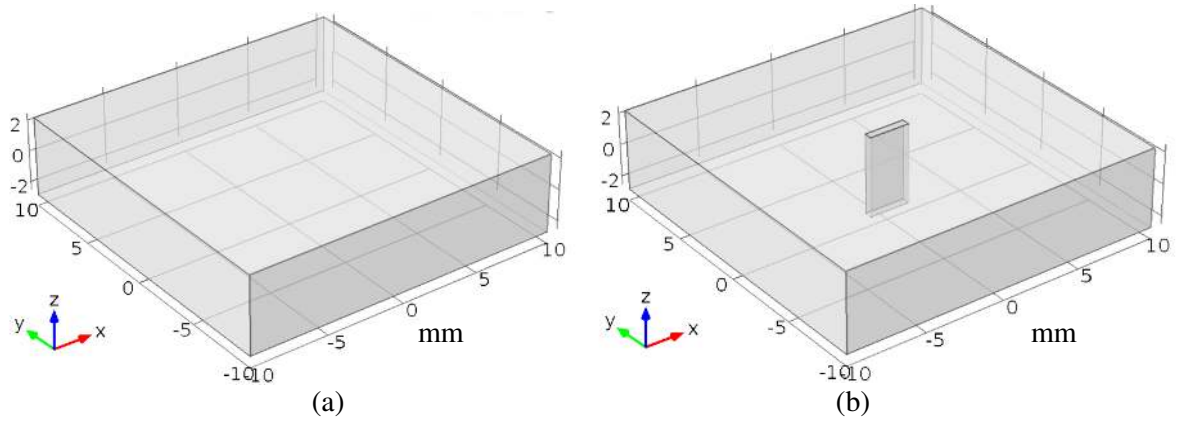

(a) (b)

Figure 1. Models verification (a) aluminium plate (b) aluminium plate with crack in the centre

In this model, the target is tested under a sweeping frequency range (1 Hz-1M Hz). The width, depth and height of the plates in (a) and (b) are 20 mm, 20 mm, and 5 mm respectively. The width, depth, and height of the simulated crack (flawed area) in plate (b) are 2.5 mm, 0.5 mm, and 5 mm respectively. Both blocks are centred at (0, 0, 0) mm. The materials of the two plates are aluminium with the conductivity of 35 M S/m at 20 degree. The exciting coil and pick-up coil with the same radius of 2 mm are both on the top of the plate with coordinates of (-1, 0, 3.5) mm and (-1, 0, 3.6) mm respectively.

C. Verification of the solver accuracy

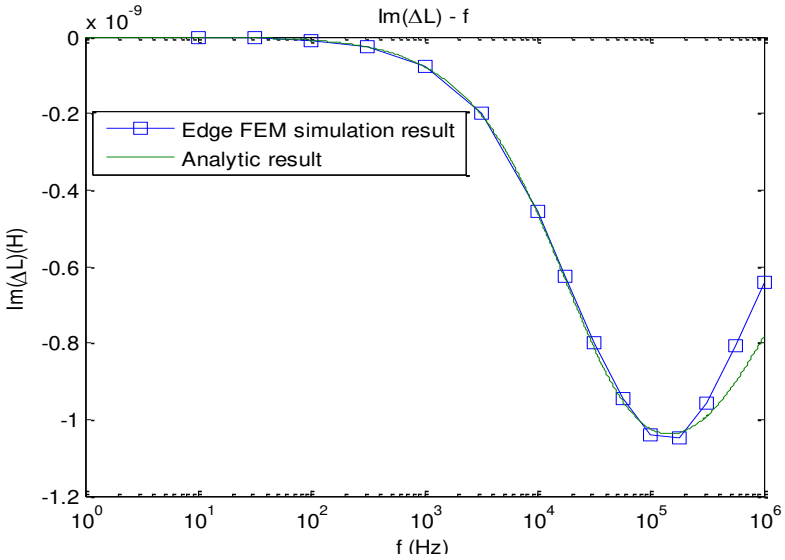

(a)

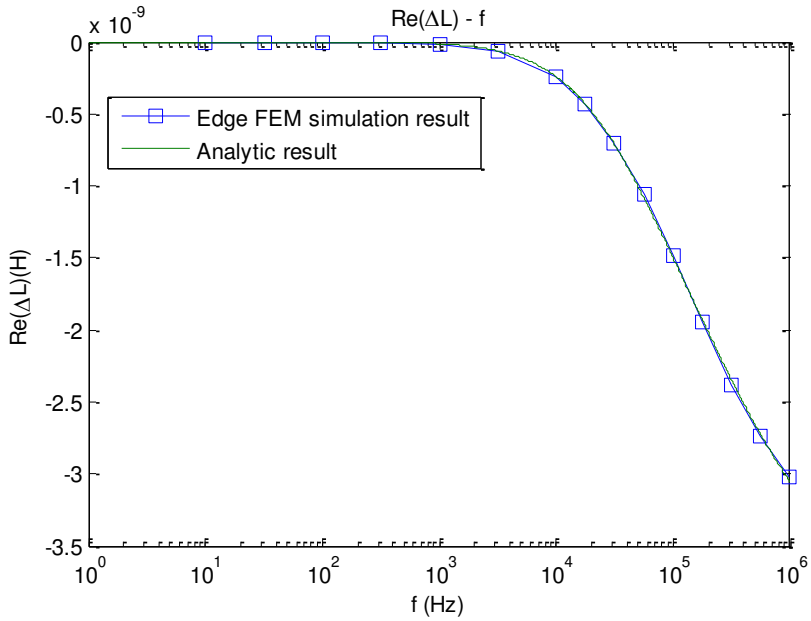

(b)

Figure 2. Inductance caused by the aluminium plate without crack (a) Imaginary part (b) Real part

The analytic solution of plate (a) inductance was calculated by the Dodd and Deeds formulas. It can be seen from Figure 2 that the error between the FEM simulation and analytic results almost can be ignored except that of the imaginary part under the frequency range from 0.1M Hz to 1M Hz, which is due to the approximating the plate as a plate with infinite length and width.

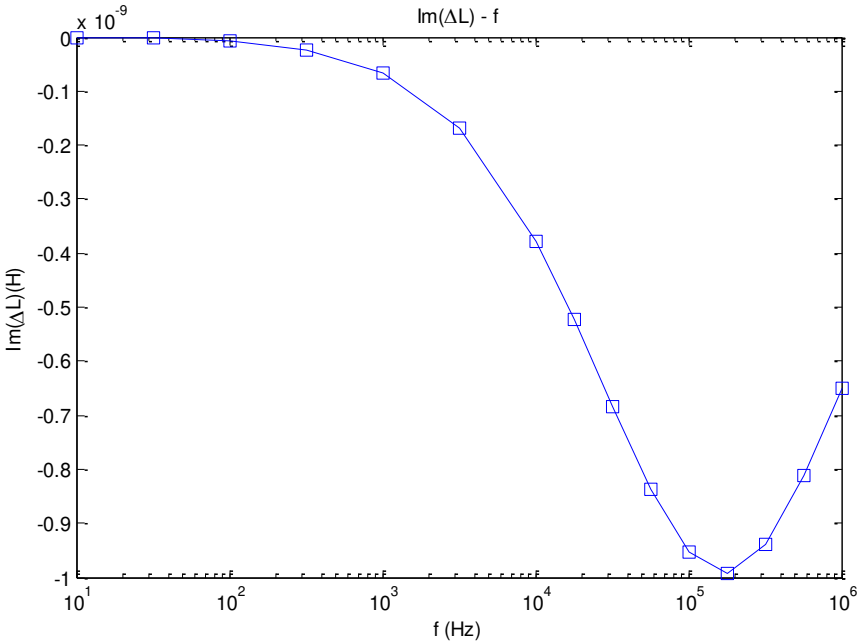

(a)

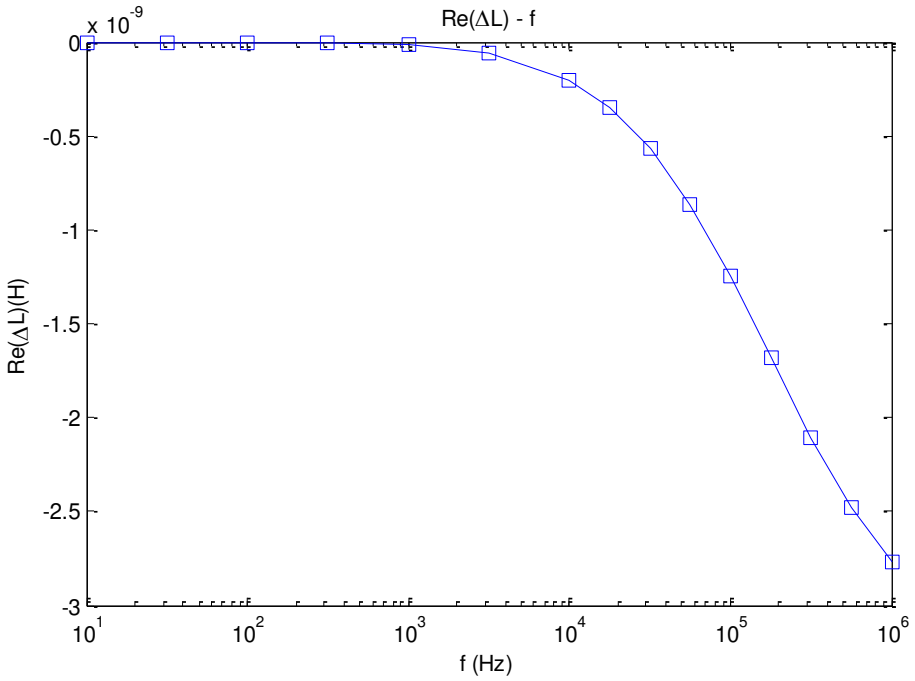

(b)

Figure 3. Inductance caused by the aluminium plate with a crack in the center (a) Imaginary part (b) Real part

Once the accuracy of edge FEM simulation was proved by comparing its results of plate (a) inductance with Dodd and Deeds method in Figure 2, the inductance results of the plate (b) can also be calculated by edge FEM simulation, as in Figure 3.

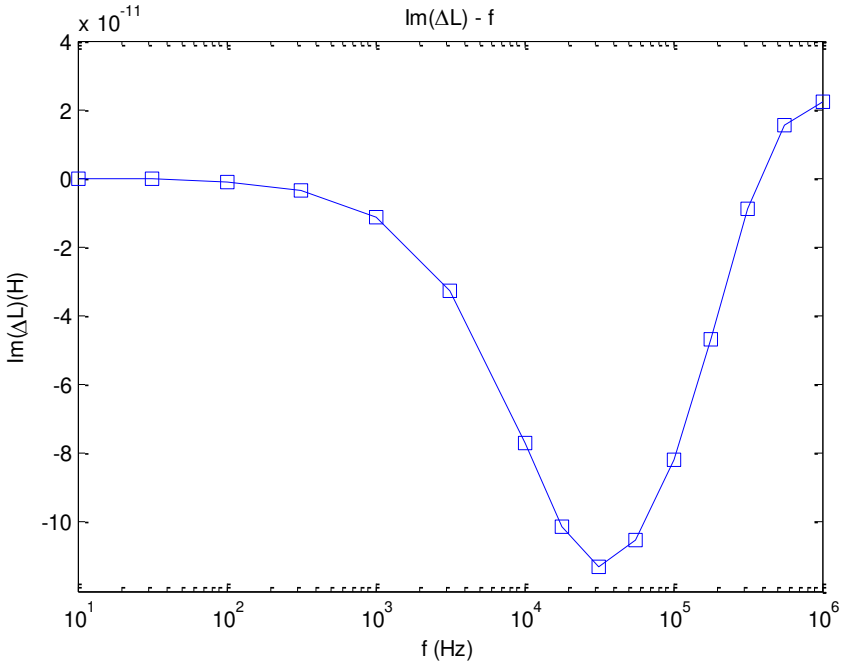

(a)

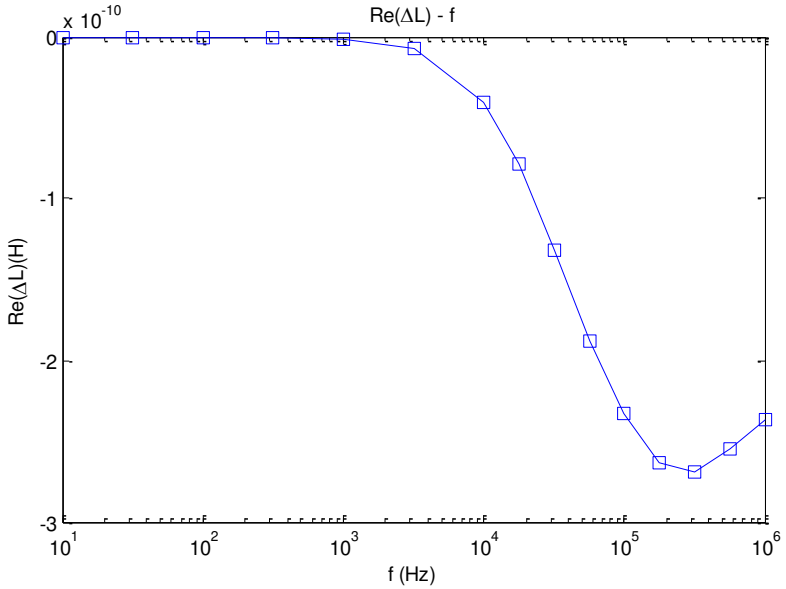

(b)

Figure 4. Inductance caused by the crack in the centre (a) Imaginary part (b) Real part

These figures show the inductance caused by the flawed area in the centre of plate (b), which is actually the same value as the subtraction of plate (a) inductance (as in figure 2) and plate (b) inductance (as in Figure 3).

D. Results

D.1. Acceleration performance

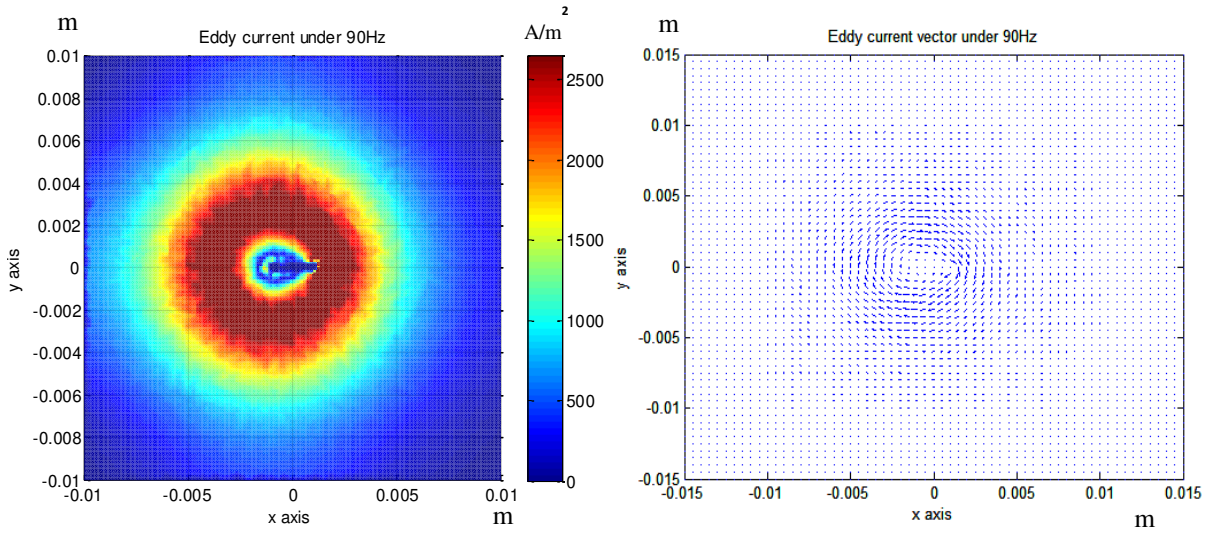

(a) (b)

Figure 5. Eddy current frames under the frequency of 90 Hz (a) Colour map (b) Quiver map

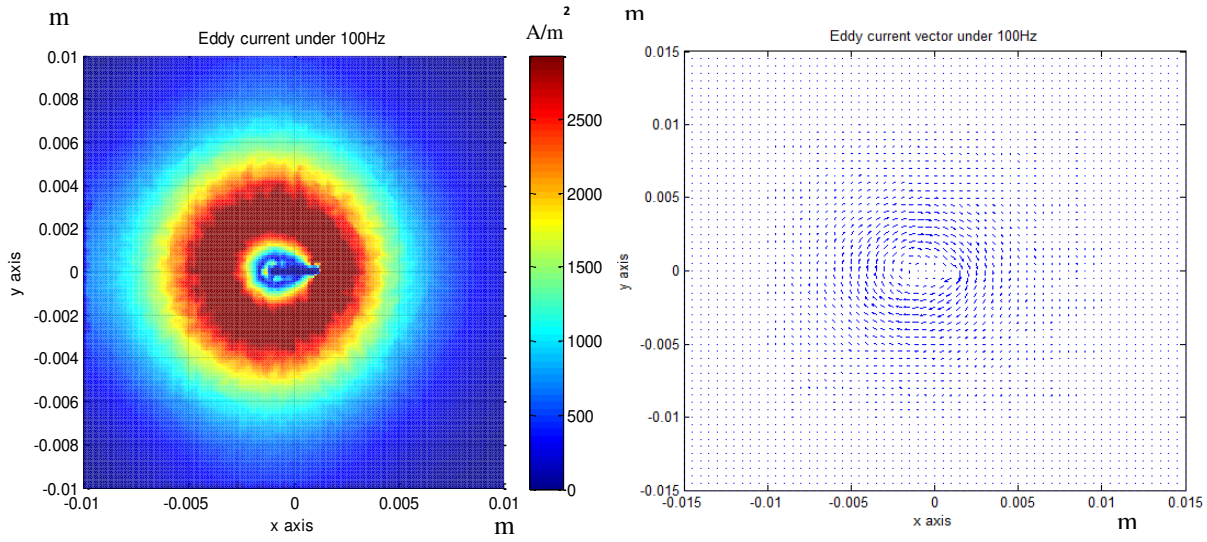

(a) (b)

Figure 6. Eddy current frames under the frequency of 100 Hz (a) Colour map (b) Quiver map

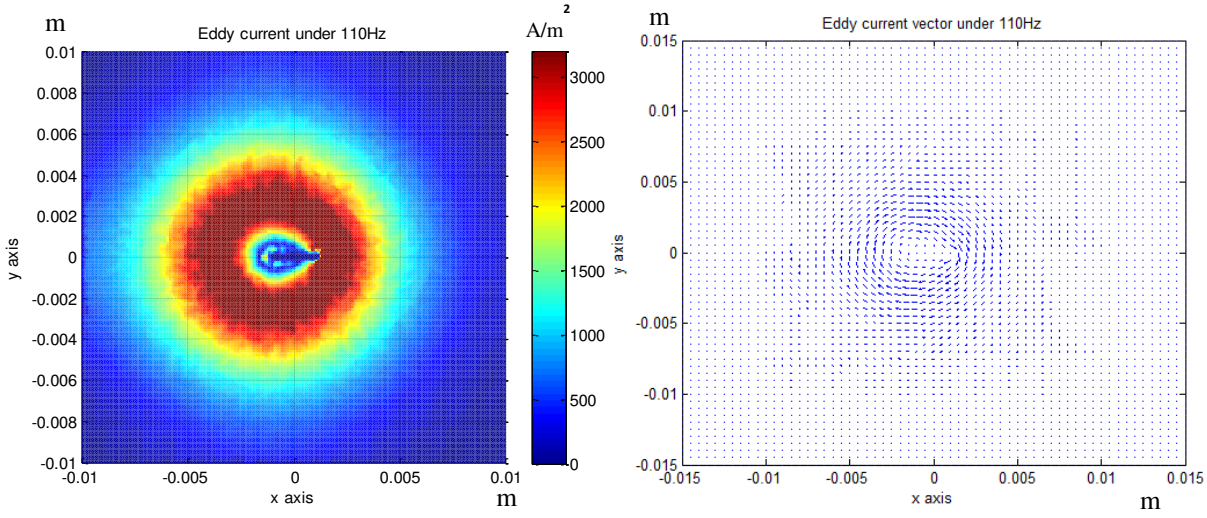

(a) (b)

Figure 7. Eddy current frames under the frequency of 110 Hz (a) Colour map (b) Quiver map

Figures 5, Figure 6, and Figure 7 illustrate both the colour maps and quiver maps of the eddy current distributions under the frequency of 90, 100, and 110 Hz. As can be seen from the legend changes on the colour map, the eddy current increases as frequency increases, but a similarity in pattern can be observed.

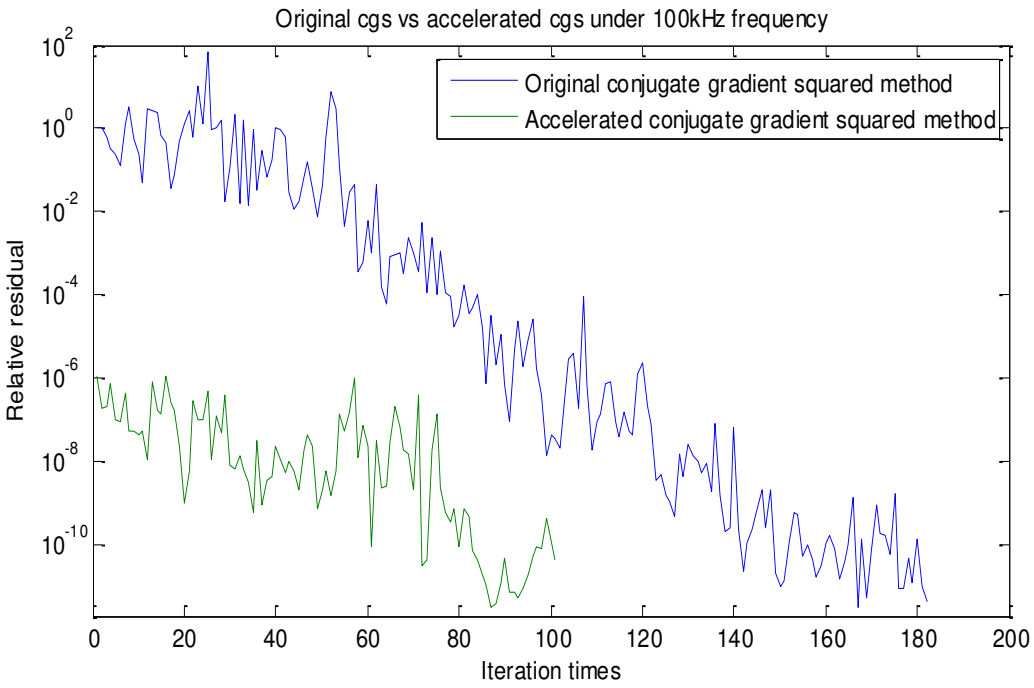

Figure 8. Convergence of original conjugate gradient squared (CGS) method compared with that of conjugate gradient squared (CGS) method with an initial guess

Figure 8 demonstrates the relative residual changes verse iteration numbers. It can be seen that the conjugate gradient squared (CGS) method with an initial guess converges much faster than the original one.

D.2. Effect of frequency step

As the solution for the previous frequency was assigned to be the initial guess of the next frequency, the similarity between the adjacent frequencies may affect the acceleration efficiency. First, the acceleration performances under the effect of different linear frequency steps were analysed.

Table1. Original and Accelerated computation time for linear frequency step of 50 Hz and 100 Hz when model (Fig. 1) is meshed into 30k elements

	frequency							
Linear frequency step of 50 Hz	10	60	110	160	210	260	310	360
Linear frequency step of 100 Hz	10		110		210		310	
Original computation time (s)	5.49	5.81	6.02	6.09	6.12	6.13	6.15	6.18
Original iteration number	399	426	431	439	442	443	445	447
Accelerated computation time with Linear frequency step of 50 Hz (s)		3.59	3.72	3.76	3.78	3.79	3.8	3.82
Accelerated iteration number with Linear frequency step of 50 Hz		198	199	201	205	206	206	207
Accelerated computation time with Linear frequency step of 100 Hz (s)			4.08		4.19		4.21	
Accelerated iteration number with Linear frequency step of 100 Hz			209		215		217	

As can be seen from Table.1, the acceleration efficiency for the linear frequency step of 50 Hz is higher than that for the linear frequency step of 100 Hz. Then it can be assumed firstly that larger frequency steps may result in lower acceleration efficiency. Further validation studies are shown as followings.

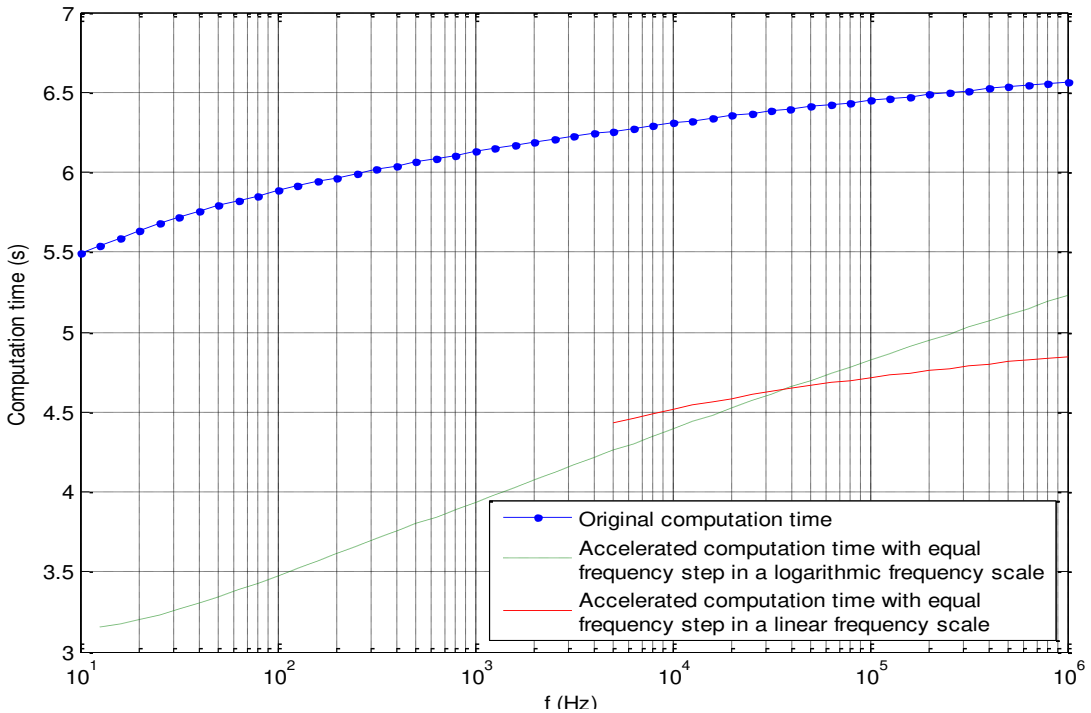

Figure 9. Original and Accelerated computation time for differet frequencies when model (Fig. 1) is meshed into 30k elements

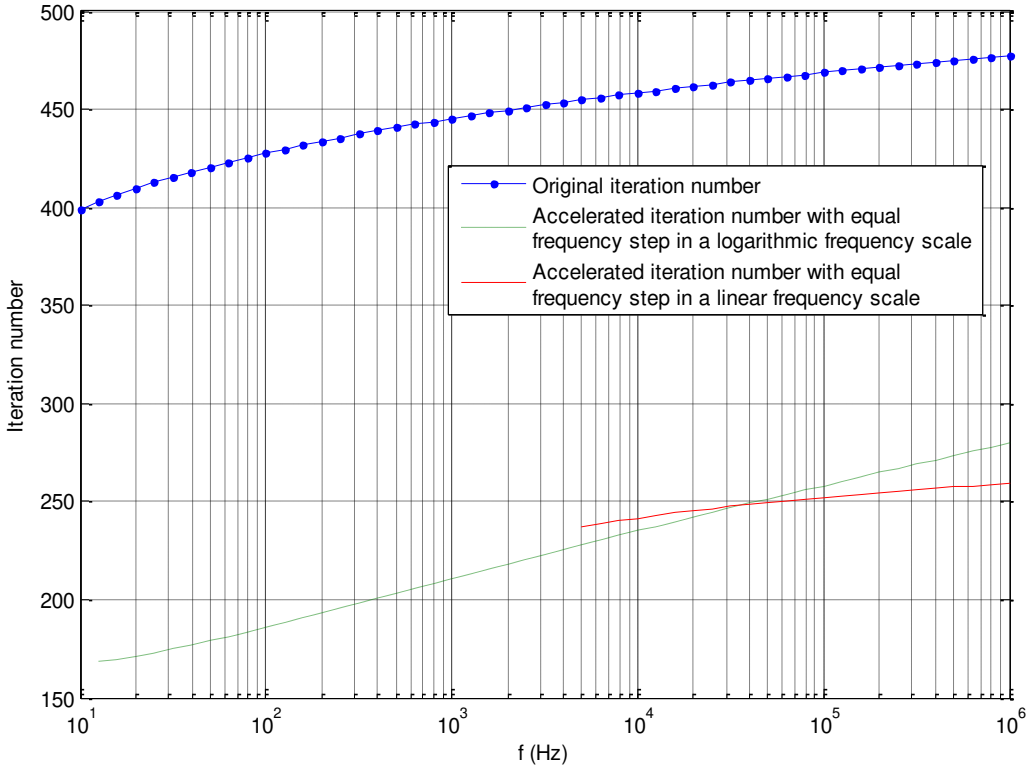

Figure 10. Original and Accelerated iterations for differet frequencies when model (Fig. 1) is meshed into 30k elements

Figure 9 and Figure 10 exhibit the computation time and iteration number before and after the acceleration with the same Maximum Interference Threshold (MAXIT) of 1.00E-14 from 10 Hz to 1 M Hz.

Equal frequency step in a logarithmic frequency scale (i.e. 10^{1}, $10^{1.2}$, $10^{1.4}$, $10^{1.6}$, $10^{1.8}$, and 10^{2} Hz between 10 Hz and 100 Hz, here we chose $10^{0.1}$ Hz for each frequency step in a logarithmic frequency scale) and equal frequency step in a linear frequency scale (5k Hz for each step) were simulated to evaluate the efficiency of the proposed method. The accelerated computation time and iteration number of 10 Hz is zero as it is the start frequency. Then, the result from 10 Hz can be used as an initial guess for the next frequency ($10^{1.2}$ Hz or 5010 Hz). The following frequencies can be treated in a similar fashion.

As can be seen from Figure 9 and Figure 10, the computation time and iterations increase slightly as frequencies rise, which is due to the skin effect and the resulted more singular system stiffness matrix with the increased frequency. And the acceleration efficiency for equal frequency step in a logarithmic frequency scale is higher than that of equal frequency step in a linear frequency scale up to 104.2 Hz, after which point, the trend reverses. This is possibly due to the larger frequency steps after 104.2 Hz on a logarithmic frequency scale.

D.3. Effect of mesh element density

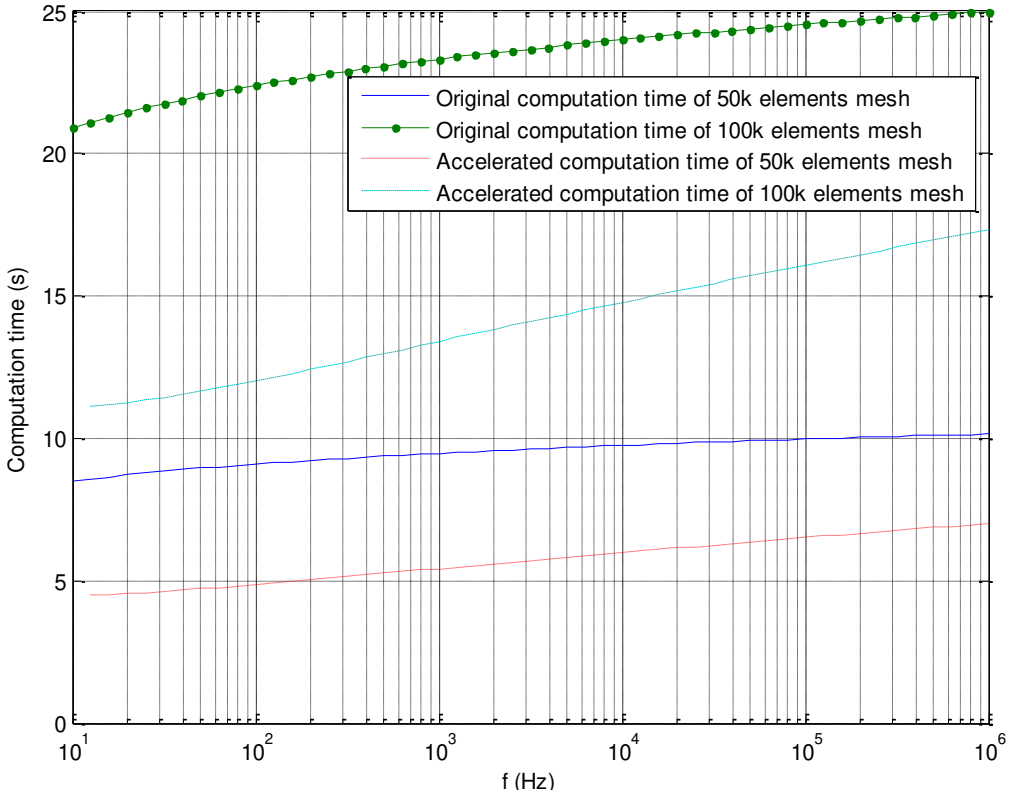

Figure 11. Original and Accelerated computation time for differet frequencies when model (Fig. 1) is meshed into 50k and 100k elements

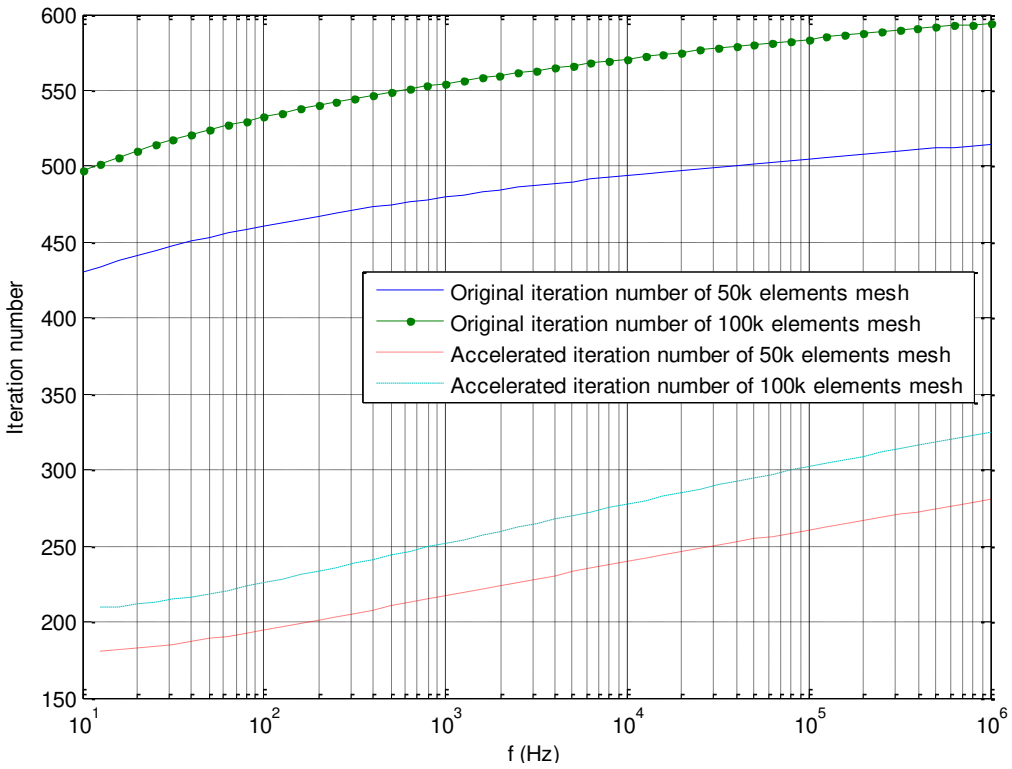

Figure 12. Original and Accelerated iterations for differet frequencies when model (Fig. 1) is meshed into 50k and 100k elements

Figure 11 and Figure 12 show the computation time and iteration number before and after the acceleration with the same Maximum Interference Threshold (MAXIT) of 0.80E-14 from 10 Hz to 1 M Hz when the model is meshed into 50k and 100k elements respectively. Equal frequency steps in a logarithmic frequency scale ($10^{0.1}$ Hz) were simulated to evaluate the efficiency of the proposed method.

It can be concluded from the above figures that the acceleration efficiency is almost immune to the mesh element density as the degree to which the improvement has been achieved remains similar irrespective of the mesh density.

We also modelled copper in addition to aluminium; the results suggest that this does not have significant effect on the efficiency of the method.

4. Conclusions

This paper has considered a method of accelerating the computation of frequency sweeping in eddy current calculation using the finite-element method (FEM). Based on the Bi-conjugate Gradients Stabilised (CGS) processing method, this method utilizes the previous adjacent computation results as the initial guess of the iteration computation for the next adjacent frequency.

Numerical tests suggest that the method can increase the speed of convergence by several folds in the tested cases. And the performance shows larger frequency step can result in lower acceleration efficiency. In the end, the acceleration efficiency of this method is proved to be immune to the mesh elements density which is because the ratio of original computation time/accelerated computation time or original iterations/accelerated iterations stay almost invariable as the model mesh element increase under the fixed frequency. Copper is also modelled in addition to aluminium; and results have not showed significant effect on the efficiency of the proposed acceleration method.

References

[1] Cekirge, H. (1988). Auxiliary source point method: the inhomogeneous and nonlinear Laplace equation. Engineering Analysis, 5(1), pp.49-52. ISSN: 0264-682X

[2] Reddy, J. N. (1993). An introduction to the finite element method. New York: McGraw-Hill ISBN: 0070513465.

[3] Margetts, Lee, Ian M. Smith, and J. Leng. "Parallel 3D finite element analysis of coupled problems." III European Conference on Computational Mechanics Solids Structures and Coupled Problems in Engineering, ECCM. 2006.

[4] Lenzi, Marcos S, et al. "A fast frequency sweep approach using Padé approximations for solving Helmholtz finite element models." Journal of Sound and Vibration 332.8 (2013): 1897-1917.

[5] Li, Y., Theodoros T., and Gui Y T. "Magnetic field-based eddy-current modeling for multilayered specimens." Magnetics, IEEE Transactions on 43.11 (2007): 4010-4015.

[6] Jin M, and Nie Z P. "FEM-DDM with an efficient second-order transmission condition in both high-frequency and low-frequency applications." Progress In Electromagnetics Research B 50 (2013): 253-271.

[7] Liu Y, Yuan J. A finite element domain decomposition combined with algebraic multigrid method for large-scale electromagnetic field computation. IEEE transactions on magnetics. 2006 Apr;42(4):655-8.

[8] Zhao K, Vouvakis MN, Lee JF. Solving electromagnetic problems using a novel symmetric FEM-BEM approach. IEEE Transactions on magnetics. 2006 Apr;42(4):583-6.

[9] Matsuoka F, Kameari A. Calculation of three dimensional eddy current by FEM-BEM coupling method. IEEE Transactions on Magnetics. 1988 Jan;24(1):182-5.

[10] Steinmetz T, Godel N, Wimmer G, Clemens M, Kurz S, Bebendorf M. Efficient symmetric FEM-BEM coupled simulations of electro-quasistatic fields. IEEE Transactions on Magnetics. 2008 Jun;44(6):1346-9.

[11] Schrefl T, Fidler J, Kirk KJ, Chapman JN. A higher order FEM-BEM method for the calculation of domain processes in magnetic nano-elements. IEEE Transactions on Magnetics. 1997 Sep;33(5):4182-4.

[12] Preda G, Cranganu-Cretu B, Hantila FI, Mihalache O, Chen Z, Miya K. Nonlinear FEM-BEM formulation and model-free inversion procedure for reconstruction of cracks using pulse eddy currents. IEEE transactions on magnetics. 2002 Mar;38(2):1241-4.

[13] Georgii, Joachim, and Rudiger W.. "A streaming approach for sparse matrix products and its application in Galerkin multigrid methods."Electronic Transactions on Numerical Analysis 37 (2010): 263-275.

[14] Fritschy, J., et al. "Using the GRID to improve the computation speed of electrical impedance tomography (EIT) reconstruction algorithms."Physiological measurement 26.2 (2005): S209.

[15] Maimaitijiang, Y., et al. "Evaluation of parallel accelerators for high performance image reconstruction for magnetic induction tomography."Journal of Selected Areas in Software Engineering (JSSE) (2011).

[16] Godel N, Schomann S, Warburton T, Clemens M. GPU accelerated Adams–Bashforth multirate discontinuous Galerkin FEM simulation of high-frequency electromagnetic fields. IEEE Transactions on magnetics. 2010 Aug;46(8):2735-8.

[17] Godel N, Nunn N, Warburton T, Clemens M. Scalability of higher-order discontinuous Galerkin FEM computations for solving electromagnetic wave propagation problems on GPU clusters. IEEE Transactions on Magnetics. 2010 Aug;46(8):3469-72.

[18] Kiss I, Gyimothy S, Badics Z, Pavo J. Parallel realization of the element-by-element FEM technique by CUDA. IEEE Transactions on Magnetics. 2012 Feb;48(2):507-10.

[19] Bíró, O. (1999). Edge element formulations of eddy current problems. Computer Methods in Applied Mechanics and Engineering. 169(3-4), pp.391-405. ISSN: 0045-7825

[20] Zeng, Z., Udpa, L., Udpa, S. S., & Chan, M. S. C. (2009). Reduced magnetic vector potential formulation in the finite element analysis of eddy current nondestructive testing. IEEE transactions on magnetics, 45(3), 964-967.

[21] Ktistis, C., Armitage, D. W., & Peyton, A. J. (2008). Calculation of the forward problem for absolute image reconstruction in MIT. Physiological measurement, 29(6), S455.

Appendix. Analytic Solution

Initially, the Dodd and Deeds analytical solution will be considered, which describes the inductance change of an air-core coil caused by a layer of non-magnetic, metallic plates [22]. Other similar formulas exist [23]. The difference in the complex inductance is $\Delta L(\omega) = L(\omega) - L_A(\omega)$, where the coil inductance above a plate is $L(\omega)$. And $L_A(\omega)$ is the inductance in free space.

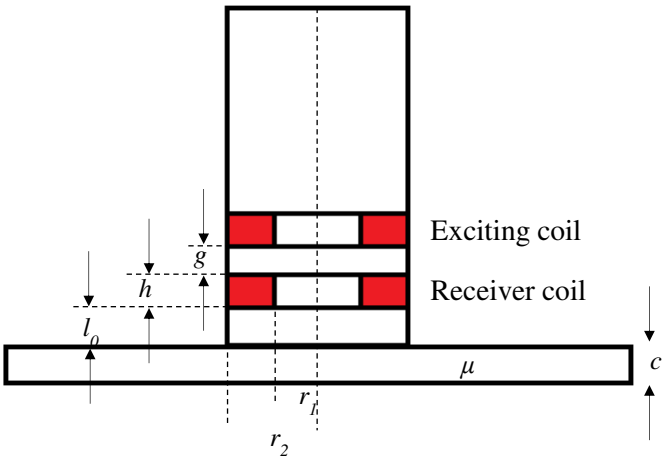

Figure 13. Sensor configuration

Table 2. Coil parameters

r_1	2mm
r_2	2.4mm
lo (lift-off)	0.2mm
h (height)	1mm
g (gap)	0.5mm
Number of turns N1 = N2	16

The formulas of Dodd and Deeds are:

$$\Delta L(\omega) = K\int_0^\infty \frac{P^2(\alpha)}{\alpha^6} A(\alpha)\phi(\alpha)d\alpha \tag{7}$$

Where,

$$\phi(\alpha) = \frac{(\alpha_1+\alpha)(\alpha_1-\alpha)-(\alpha_1+\alpha)(\alpha_1-\alpha)e^{2\alpha_1 c}}{-(\alpha_1-\alpha)(\alpha_1-\alpha)+(\alpha_1+\alpha)(\alpha_1+\alpha)e^{2\alpha_1 c}} \tag{8}$$

$$\alpha_1 = \sqrt{\alpha^2 + j\omega\sigma\mu_0} \tag{9}$$

$$K = \frac{\pi\mu_0 N^2}{h^2(r_1-r_2)^2} \tag{10}$$

$$P(\alpha) = \int_{\alpha r_1}^{\alpha r_2} xJ_1(x)dx \tag{11}$$

$$A(\alpha) = \mathrm{e}^{-\alpha(2l_0+h+g)}(\mathrm{e}^{-2\alpha h}+1) \tag{12}$$

μ_0 denotes the permeability of free space. N denotes the number of turns in the coil; r_1 and r_2 denote the inner and outer radii of the coil; while l_0 and h denote the lift-off and the height of the coil; and c denotes the thickness of the plate.

[22] Dodd C V, Deeds W E. Analytical solutions to eddy-current probe-coil problem. J. Appl. Phys., 1968 39, 2829–2839.

[23] Burke S K and Ditchburn B J, Mutual Impedance of Planar Eddy-Current Driver-Pickup Spiral Coils, Research in Nondestructive Evaluation 19: 1-19, 2008.